Preparation and thermodynamic analysis of the porous ZrO_2/(ZrO_2+Ni) functionally graded bolted joint

Wenbin Zhou[a,*] et al.

[a]*State Key Lab for Turbulence and Complex Systems, College of Engineering, Peking University, Beijing, 100871, China*

[b]*Department of Mechanics, Beijing Jiaotong University, Beijing, 100044, China*

[c]*National Center for Nanoscience and Nanotechnology, Beijing, 100190, China*

Abstract

Ceramic-metal functionally graded materials (FGMs) have been extensively used in aerospace engineering where high strength and excellent heat insulation materials are desired. In this paper, the thermodynamic behavior of the Thermal Protection System (TPS) used bolted joints made up of porous ZrO_2/(ZrO_2+Ni) FGMs is investigated by finite-element (FE) modeling. The bolted joint is subjected to reentry heating corresponding to the Access to Space Vehicle. Thermodynamic simulations are carried out to yield the transient response of the porous ZrO_2/(ZrO_2+Ni) functionally graded bolted joint (FGBJ). The effects of the preload on the thermomechanical behavior and service reliability of the bolted joint are numerically analyzed in detail by ABAQUS codes. It is found that the preload relaxation of the bolted joint occurs at elevated temperature, and the preload has significant influence on service reliability of the bolted joint under transient thermomechanical circumstances. With the increase of the preload, stress concentration which occurs at the root of the first thread of the bolt increases rapidly and predominates in service reliability. Proper preload is thus defined to balance the service reliability and tightness of the bolted joint. Further studies show that the shape of the nut has a great effect on the stress concentration of the thread, the optimized nut is designed to reduce the stress concentration of the thread, and thus the reliability of the bolted joint is also improved.

Keywords: A. Ceramic-matrix composites (CMCs); B. Thermomechanical; C. Finite element analysis (FEA); E. Joints/joining

[*] Corresponding author. Tel.: +86 010 62757417
Email address: sgai@pku.edu.cn and mjchen81@gmail.com.

1. Introduction

Thermal Protection System (TPS) is usually covered on the surface of the aircraft as the thermal protecting layer. Due to the complex shape and structure of the aircraft, a unibody design and manufacture of TPS is infeasible, therefore it is unavoidable to connect lots of thermal protection components. As a result, heat shorts caused by the gap and joints between thermal protection components cannot be ignored [1]. Heat shorts may lead the interior part of the fuselage structure to an extreme high temperature, severely influencing the heat insulation property of the TPS. In the process of service, the TPS has to withstand not only thermal loads, but also mechanical loads as well as harsh chemical environments, repeatedly without failure [2]. Therefore, in the study of the TPS, the analysis of heat shorts effect and the use of high temperature resistant joints with high strength are indispensable.

Many efforts have been done on metallic thermal protection system, including the design and characterization of thermal insulation material/structure [3-8], however, heat shorts blocking joints have been rarely studied. Also, most researches focused on metal joints [9-15], which had quite poor heat insulation properties. Some studies were carried out on C/SiC joints [16-18], yet the complicated fabrication approaches for geometrically complex composites such as bolted joints have certain limitations in terms of size and shape, which have greatly limited their wider applications. The studies for the thermodynamic properties of these joints which are quite necessary for joints used on TPS are less. Functionally graded materials (FGMs) are ideal candidates for the applications requiring multifunctional performance. For example, the ceramic-metal FGMs can be designed to take advantages of the mechanical strength of metals and the heat and corrosion resistance of ceramics [19-20]. In our previous work, we fabricated and experimentally investigated the microstructure and thermomechanical properties of the porous ZrO_2/(ZrO_2+Ni) ceramics and found that they had a low thermal conductivity and high strength [21-22]. Therefore, the ceramic-metal FGMs can be a potential candidate for heat shorts blocking joints. However, most of the FGMs have thermal stress due to a gradually macroscopic change in composition, which are destined to affect the mechanical property and service reliability of the FGMs [23-24]. Also, the preload is an important factor that cannot be neglected. On the one hand, the preload can enhance the reliability and tightness of bolted joints. On the other hand, the preload may cause the fracture of bolted joints in advance under thermomechanical circumstances. So it is of great importance to study the thermodynamic properties of bolted joints made up of ceramic-metal FGMs, which will guide the preload and structure design of joints. Finite element analysis (FEA) has been widely used to analyze the thermal and thermomechanical properties of various materials and structures [25-29], since the method through experimental study to obtain the thermomechanical properties of the ceramic-metal functionally graded bolted joint (FGBJ) is accurate but time-consuming, so the theoretical simulation and optimization would be rather important for the successful implementation of ceramic-metal functionally graded jointing technology in a wide variety of high temperature application.

In this paper, firstly a thermomechanical coupled model is constructed to study the thermodynamic properties of the ceramic-metal functionally graded bolted joint (FGBJ), whose material systems (porous ZrO_2/(ZrO_2+Ni) FGMs) are fabricated by cold isostatic pressing and pressureless sintering (CIP-PLS). Microstructures and mechanical properties of the FGMs are experimentally studied in our previous work [21-22]. Then the heat transfer and thermomechanical responses are investigated under different preloads to study the service reliability of the bolted joint. The effects of the preload on the thermomechanical responses and service reliability of the bolted joint are analyzed in detail, thus the proper preload is proposed to balance the service reliability and tightness of the bolted joint. Finally the optimal structural design of the bolted joint under thermomechanical circumstances is done to improve the service reliability. The findings will highlight the optimization of the preload and the structure of the bolted joint.

2. Materials and structure of the bolted joint

Porous ZrO_2/(ZrO_2+Ni) functionally graded samples are fabricated, with the height of the bearing load layer (layer a, 12% porosity), transition layer (layer b, 15% porosity) and middle layer (layer c, 30% porosity) being l_a=10mm, l_b=2mm, and l_c=10mm in the axial direction, respectively (see Fig. 1). These samples are further manufactured into the functionally graded bolted joints. The materials and structure of the bolted joint are shown in Fig. 2. The bolt thread, bolt head and nut are all comprised of the bearing load layer (ZrO_2+30 vol. %Ni) to ensure the mechanical strength and service reliability. The bolt shank without threads is mainly composed of the middle layer (ZrO_2), which serves the purpose of heat resistance. The transition layer (ZrO_2+15 vol. %Ni) on the bolt shank is designed to reduce the residual stresses which are generated inevitably due to the mismatch in coefficients of thermal expansion between different layers. The transition layer also serves the purpose of cutting the fillet. According to the standard handbook of fastening and joining [30], the diameter and height of the bolt head are s=12.8mm and k=5.5mm, respectively. The diameter of the bolt shank is D=7.8mm, which is also the major diameter of the external thread. The thread pitch is p=1.25mm. The height and diameter of the nut are m=6.8mm and s=13mm, respectively. The number of threads on the nut is thus calculated to be five. In this study, the number of threads is not a significant factor because stress concentration at the roots of the threads is found to vary little after the first three threads. The thread class used in this study is class 3A and

3B for external and internal threads respectively, since this class of thread is most used in high-precision applications. The root radius for the threads is taken as $L/6$, where L is the thread height [30]. The bolted joints with the preload are called high-strength bolts, which usually need only 2~3 threads out of the nut when the bolt and nut are fully engaged. Therefore, we suppose the number of threads on bolt shank is eight, and the height of the bolt shank with threads is accordingly to be b=10mm.

3. Numerical Modeling and Finite Element Analysis

3.1. Finite element model

To study the thermomechanical behaviors of the bolted joint, a two-dimensional (2D) axisymmetric finite element model is constructed based on ABAQUS code using the advantage of symmetry, as illustrated in Fig. 3. The error resulting from modeling the bolt and nut axisymmetrically and neglecting the helix angle is ignored in this study, since the helix angle is very small (less than 2 deg) on most bolts and thus the three-dimensional effect can be neglected. In fact, the 2D approximation for such a problem was also adopted in the earlier experimental photoelastic studies [31]. The model consists of 48147 elements with 48976 nodes. The finite element mesh is refined using a very small element length at the crest and root of the threads. The nodes between two mutually contacted threads are coincident to improve the convergence. The thermomechanical response of the system is obtained in two steps. First, the heat transfer problem is solved to obtain the time-dependent temperature distribution in the bolted joint due to the applied thermal loads and boundary conditions. Next, the thermal stresses caused by the temperature distributions are determined. The solutions are facilitated by using the same mesh for both the heat transfer and thermal stress problems. The DCAX4 elements are used for the heat transfer analysis and the CAX4 elements for the thermal stress analysis.

The material parameters (mechanical properties and thermal properties) used in the numerical simulations are listed in Table 1-2. It should be noted that, the material parameters for ZrO_2 and Ni were only experimentally tested at some discrete temperature points, while the parameters that have not been measured at other temperatures will be given by interpolation in the simulations. The material constants in each composition, such as elastics modulus, thermal conductivity, coefficient of thermal expansion (CTE), specific heat and Poisson's ratio are calculated as follows [32-33]:

$$\left.\begin{aligned} E &= \frac{8E_0(1-P)(1+\mu_0)(23+8\mu_0)}{8(1+\mu_0)(23+8\mu_0)+P(5+\mu_0)(37-8\mu_0)} \\ C &= C_0 \quad , \quad \alpha = \alpha_0 \quad , \quad \mu = \mu_0 \\ \lambda &= \frac{\lambda_0[(1-P)^{2/3}\lambda_0 + P^{2/3}\lambda_g]}{P^{1/3}\lambda_0 + (1-P)^{1/3}[(1-P)^{2/3}\lambda_0 + P^{2/3}\lambda_g]} \end{aligned}\right\} \quad (1)$$

where P is the porosity, λ_g is the thermal conductivity of air, E_0, C_0, α_0, μ_0 and λ_0 are all dependent on the ceramic volume fraction and can be expressed from the Vegard's rule below [34]:

$$\left.\begin{aligned} M_0 &= M_{ce}V_{ce} + M_m V_m \\ \lambda_0 &= \lambda_{ce}[1+\frac{3(\lambda_m-\lambda_{ce})}{3\lambda_{ce}+(\lambda_m-\lambda_{ce})(1-V_m)}] \end{aligned}\right\} \quad (2)$$

where M represents the material property parameters (E , α , C , μ and ρ), V_{ce} donates the ceramic volume fraction, and subscripts '*ce*' and '*m*' represent ceramic and metal, respectively.

The material model used is based on the tension experiment of the porous ZrO_2/(ZrO_2+Ni) FGMs. The tensile stress-strain relationship is show in Fig. 4. It should be noted that, the stress and strain obtained by experimental test are only the nominal stress and nominal strain, which should be transformed into the true stress and true stain used in ABAQUS. The plastic strain which is input into ABAQUS is calculated as

$$\varepsilon_{pl} = \left|\ln(1+\varepsilon_{nom})\right| - \frac{\left|\sigma_{nom}(1+\varepsilon_{nom})\right|}{E} \quad (3)$$

where E is the Young's modulus, ε_{pl} , σ_{nom} , ε_{nom} are the plastic strain, the nominal stress and nominal stain, respectively.

3.2. Simulation process

Firstly, the heat transfer simulations are carried out to obtain the time-dependent temperature distribution in the bolted joint. The initial temperature of the specimen is 25ºC (i.e., room temperature), the ambient air temperature of the top and bottom surfaces of the bolted joint are set as 1200ºC and 25ºC, respectively. The temperature dependent convection and radiation coefficients can be seen in Table 1. The total loading time is 1000 s. The transient temperature distribution is then computed.

After the heat transfer process, a coupled thermal-mechanical approach based on ABAQUS nonlinear finite element codes is adopted. Contact is defined between all the contacted surfaces. The friction coefficient of bolted joints usually ranges from 0.1~0.2 [35], and thus the same friction coefficient 0.15 is adopted here between all the contacted surfaces. The axis of symmetry of the bolt is restrained in the radial direction. The upper surface of the nut contacted with the plate is restrained in the horizontal y direction, while the lower surface of the nut is free. A surface pressure of *F*=100MPa is applied to the top surface of the bolt head. The preload is applied to the bolt through the bolt load method in ABAQUS. It should be noted that, the loads are applied gradually (little loads are applied initially) and the constraints are released stepwise (extra constraints are needed initially) to realize the convergence. The thermal load is applied by importing the transient temperature distribution calculated from the heat transfer process. The thermomechanical coupling studied here is conducted by applying the mechanical load and thermal load simultaneously, which is called transient thermodynamic behavior.

4. Results and Discussion

4.1. Heat transfer

Heat transfer behaviors of the bolted joint in 1000s are numerically simulated and the temperature contour of the bolted joint at the end of the heat transfer is shown in Fig. 5a. The results show that the temperature of the top surface of the bolt at 1000s is approximately equal to the top surface ambient air temperature (1200ºC). The temperature decreases along the height direction of the bolt. The bottom surface temperature of the bolt is about 150ºC at 1000s, which has 125ºC increase compared with the original temperature. Fig. 5b illustrates the temperature history of the bolt at different locations, i.e. the top surface of the bolt, the bottom surface of the bolt, the upper (left) surface of the middle layer (ZrO_2), the center of the middle layer (ZrO_2) and the lower (right) surface of the middle layer (ZrO_2). As shown in Fig. 5b, temperatures at different locations increase monotonously with time initially, and then reach the steady state almost at the same time 500s. The steady temperatures of the upper (left) and lower (right) surfaces of the middle layer (ZrO_2) are 1029ºC and 397ºC, respectively. Compared with the steady temperatures of the top surface (1190ºC) and bottom surface (125ºC) of the bolt, it is clear that the middle layer (ZrO_2) plays a dominant role in the heat resistance. This is because that the conductivity of ZrO_2 is lower than that of the upper-layer material (ZrO_2+30vol. %Ni). As listed in Table 1, through Eq. (1) and (2), the conductivity of the upper-layer material (ZrO_2+30vol. %Ni) is approximately 3~4 times greater than that of ZrO_2. The equivalent heat resistance schematic of the bolt in the height direction is shown in Fig. 6. By Fourier's law of heat conduction, the equivalent conductivity of the bolt in the height direction can be approximately calculated as [36]:

$$\lambda_{eff} = \frac{L}{AR} \quad (4)$$

where *L*, *A* are the equivalent height and cross-sectional area of the bolt correspondingly, R is the equivalent heat resistance. The heat resistance R_i of each layer is given by

$$R_i = \frac{l_i}{A_i \lambda_i} \quad (5)$$

where l_i , A_i , λ_i are the height, cross-sectional area and conductivity of each layer, respectively. The equivalent model of the whole bolt can be assumed as the series model. The equivalent heat resistance *R* and equivalent length *L* of the whole bolt can then be given by

$$\left.\begin{array}{l} L = \sum_i l_i \\ R = \sum_i R_i \end{array}\right\} \quad (6)$$

Combining Eq. (4)-(6), the equivalent conductivity of the bolt in the height direction is expressed as

$$\lambda_{eff} = \frac{\sum_i l_i}{\sum_i \frac{l_i}{\lambda_i}} \quad (7)$$

Besides the lower conductivity, the height of the ZrO_2 layer is also an important factor influencing λ_{eff} . $\frac{l_i}{\lambda_i}$ of the porous ZrO_2 layer is much greater than other layers, so the middle layer (porous ZrO_2) plays a dominant role in the heat resistance. λ_{eff} of the functionally graded bolt is 1.54 W/(m·K), while λ_{eff} of the corresponding pure ZrO_2 bolt (30% porosity of layer a, without the addition of metal phase to layer b and layer c) is 1.40 W/(m·K). The addition of metal phase to improve thermal conductivity of the functionally graded bolt is very limited.

4.2. Thermodynamic behavior

4.2.1 Preload relaxation of bolted joints

To study the variations of the preload at elevated temperature, only the thermal load is applied during 0-1000s by importing the transient temperature distribution calculated from the heat transfer simulations. The mechanical load (top surface pressure) is applied after the temperature distribution in the bolt gets steady (i.e. after 1000s), and the total loading time is 2000s. Different preloads (15, 33.5 and 50MPa) are applied to the bolted joint at the beginning of the simulation. For high strength bolts, based on the standard manual, the maximum preload is less than half of the tensile strength at room temperature. In this study, the maximum preload is set as 50MPa, which is approximately 0.3 times of the tensile strength at room temperature (168.6MPa). The axial stress-loading time curves under different preloads are illustrated in Fig. 7, taking location A as an example. A is located in the center of the middle layer (ZrO_2). Fig. 7 shows that, as the heat transfer proceeds, the axial stresses under different preloads quickly reach the maximum value almost at the same time (*t*=100s), then gradually decrease to the same value at the end of the heat transfer process. To illustrate this phenomenon, the axial stress at location A without preload is also plotted in Fig. 7, which is also called the axial thermal stress because there is no preload in this situation. As shown in Fig. 7, the axial stress with preloads has the same variation trend as the axial thermal stress. Therefore, the maximum value of the axial stress is the result of the maximum thermal stress. For different preloads, the thermal stress gets the peak value at the same time (t=100s), so the axial stress under different preloads reaches the maximum value simultaneously. The thermal stress gets the maximum value when t=100s because the temperature difference between different layers at this time is the greatest. As shown in Fig. 5b, the temperature of the top layer increases much quickly than that of the middle layer (ZrO_2). The temperature difference between these layers quickly increases as the heat transfer proceeds, reaching the maximum at almost t=100s. Then it gradually decreases and becomes constant as the heat transfer become steady after t=400s. The thermal stress also become constant after t=400s, which is the same trend as the temperature difference. From the simulation results it is learned that, preload relaxation of the bolted joint happens at elevated temperature, the preload gradually decreases in the heat transfer process and will decrease to a near zero value if the heat conduction process is sufficient.

4.2.2 Transient thermodynamic behavior

The thermal load is applied during 0-1000s by importing the transient temperature calculated from the heat transfer simulation, and is kept constant after 1000s. The mechanical load (top surface pressure of 100MPa) is applied simultaneously with the thermal load. To study the effects of the preload on the thermodynamic responses and service reliability of the bolted joint, different preloads are applied to the bolted joint at the beginning of the simulation. The most potential dangerous locations of the bolted joint are the interface between the bearing load layer (ZrO_2+30 vol. %Ni) and the transition layer (ZrO_2+15 vol. %Ni), and the root of the first thread, which are shown in Fig.5a and are marked as location B and C. This is because the residual thermal stress at location B is the maximum tensile stress, which can be seen in our previous work [22]. Besides, stress concentration is the most severe at location C. In the present work, we only give results of three representative situations, namely, Little preload (15MPa), Critical preload (33.5MPa) and Big preload (50MPa). For each situation, the axial stresses at some key locations, such as B and C, are particularly investigated. The axial stress-time curves are illustrated in Fig. 8-10.

Figure 8a-b plot the axial stress-loading time curves of location B and C under Little preload (15MPa). The corresponding temperature-time and strength-time curves are also plotted as comparison. Here, if the axial stress exceeds the material strength, the bolt is assumed to fail. In the loading process, the axial stress increases with the increment of temperature, while the material strength decreases with the increment of temperature. So, the bolt will failure when the local axial stress exceeds the strength of the local material. As shown in Fig. 8a-b, material failure at location B happens when *t*=263s, while it occurs at location C at the time *t*= 284s. Therefore, when Little preload (15MPa) is applied, thermal stresses dominate the service reliability of bolted joints. The most dangerous location of the bolt is at the interface between the bearing load layer (ZrO_2+30 vol. %Ni) and the transition layer (ZrO_2+15 vol. %Ni), where the thermal stress is the maximum tensile stress.

As the preload increases, the axial stress at location C increases much more rapidly than that of location B because of the existence of stress concentration at location C, so there should have a critical preload when material failure at location B and C happens at the same time. Under the Critical preload, the bolt joint will play the best performance and a key of this simulation in the present work is to find out the Critical preload based on a certain bolt. The axial stress-loading time curves of location B and C under Critical preload (33.5MPa) are shown in Fig. 9a-b. It should be noted that this Critical preload is identified by a series of continuous simulations with different preloads increasing from Little preload (15MPa) to Big preload (50MPa). As illustrated in Fig. 9a-b, failure almost happens simultaneously at location B and C when *t*= 221s under the Critical preload. Therefore, it is clear that the preload has significant influence on the service reliability of the bolted joint under transient thermomechanical circumstances. Stress concentration occurring at the root of the first thread of the bolt increases rapidly and predominates in the service reliability of the bolted joint with the increase of the preload. Proper preload is thus defined to be this Critical preload to balance the service reliability and tightness of bolted joints. To verify the correctness of this conclusion, the axial stress-loading time curves of location B and C under Big preload (50MPa) are shown in Fig. 10a-b. As shown in Fig. 10a-b, failure keeps occurring at location C when the preload exceeds the Critical preload, and with the increase of the preload, failure of the bolt happens earlier and earlier, that is, the service reliability of the bolted joint decreases.

4.3. Stress concentration

Stress concentration occurring at the thread root predominates the service reliability of the bolted joint. In this section, the stress concentration of the porous ZrO_2/(ZrO_2+Ni) functionally graded bolt under transient thermomechanical circumstances is studied and compared with that of the pure ceramic (ZrO_2) bolt. The thermal load is applied during 0-1000s by importing the transient temperature calculated from the heat transfer simulations, and is kept constant from 1000 to 2000s. The mechanical load (top surface load of 1000N) is applied simultaneously with the thermal load. The preload is 33.5MPa for the functionally graded bolt, and no preload is applied to the ZrO_2 bolt. Stress concentration factor is defined as the ratio of maximum axial stress in the nut-bolt system to the nominal axial stress in the shank of the bolt. Fig. 11 shows the axial stress contour of the functionally graded bolt and ZrO_2 ceramic bolt at the end of the thermomechanical process. The axial stress decreases progressively from the first thread to the subsequent threads. Dividing the top surface load (1000N) by the corresponding cross-sectional area, the nominal axial stress in the shank of the bolt is calculated as 20.9MPa, so the maximum stress concentration factor occurring at the root of the first thread of the functionally graded bolt and ZrO_2 ceramic bolt is 7.22 and 8.86, respectively. It is clear that the maximum stress concentration factor of the functionally graded bolt is reduced compared with that of ZrO_2 ceramic bolt. Since stress concentration occurring at the root of the first thread of the bolt predominates the service reliability of the bolted joint, the service reliability of the functionally graded bolt is improved compared with that of ZrO_2 ceramic bolt. It is because the addition of metal phase to threads of the functionally graded bolt can release the stress due to plastic deformation. The maximum axial stress-loading time curves of the ZrO_2 ceramic bolt under different preloads are illustrated in Fig. 12. As shown in Fig. 12, even under very little preload, the axial stress grows rapidly and even reaches the limit strength at the initial loading process because of the stress concentration at the first thread. Hence, almost no preload is able to be applied on the pure ceramic bolt, which makes it vulnerable to looseness under thermodynamic circumstance. The service reliability of the pure ceramic bolt is therefore lower than that of the functionally graded bolt.

Stress concentration can greatly degrade the high-temperature mechanical performance. S. Venkatesan's research showed that grooves on the nut can significantly reduce the stress concentration factor and improve the mechanical performance [37], but whether it is effective under high temperature still needs to be studied. Inspired by S. Venkatesan's research, an internal groove and an external groove are constructed on the nut and studied under transient thermomechanical circumstance, as shown in Fig. 13-14. The one without a groove is also plotted as comparisons. Three different cases are simulated for the functionally graded bolted joint with an internal groove. (i) b/l=1/4, (ii) b/l=2/4, (iii) b/l=3/4, where b and l are the width of the nut after and before grooving. The depth of the internal groove is fixed at $a=p/4$, where p=1.25mm is the thread pitch. As shown in Fig. 13, the maximum stress concentration factor still occurs at the root of the first thread, and gradually decreases as the decrease of b/l. When b/l=1/4, the maximum stress concentration factor decreases to 5.79 for the functionally graded bolt. Compared with the bolted joint without the groove, the maximum stress concentration factor of the functionally graded bolt decreases by 19.81%. Four different cases are simulated for the functionally graded bolted joint with an external groove, (i) a/h=1/4, b/l=2/3, (ii) a/h=1/4, b/l=5/6, (iii) a/h=1/2, b/l=2/3, (iv) a/h=1/2, b/l=5/6. It is clear from Fig. 14 that the maximum stress concentration factors all have a decrease for the four cases. When a/h=1/4, b/l=5/6, the maximum stress concentration factor decreases to 5.03 for the functionally graded bolt. Compared with the bolted joint without the groove, the maximum stress concentration factor for the functionally graded bolt decreases by 30.33%. Comparing the internal groove with the external groove, the nut with an external groove (a/h=1/4, b/l=5/6) acts best performance to reduce the stress concentration of the thread and achieves the best reliability of the joints. Therefore, the shape of the nut has a great effect on the stress concentration of the bolted joint. Both the internal and external groove can make the loading position of the nut stretches outward along the radial direction, which makes the nut bear the bending moment in an anticlockwise direction (M_z , based on the coordinate system shown in Fig. 3). Hence, the contact tightness between the first thread of the bolt and the nut decreases, while the contact tightness between the last thread of the bolt and the nut increases, resulting in the decrease of the maximum stress concentration factor at the first thread.

5. Conclusions

Thermodynamic behavior and service reliability of the Thermal Protection System (TPS) used bolted joints made up of porous ZrO_2/(ZrO_2+Ni) FGMs are numerically analyzed in detail by ABAQUS codes. From the numerical simulations some conclusions can be drawn:

(1) The middle layer (porous ZrO_2) plays a dominant role in the heat resistance of the functionally graded bolt. The addition of metal phase will obviously improve the mechanical performance of the bolted joint while it to improve thermal conductivity of the bolt is very limited.

(2) Preload relaxation of the bolted joint happens at elevated temperature. The preload decreases gradually as the heat transfer proceeds and it reaches a near zero value if the heat conduction process is sufficient.

(3) Preload has significant influence on the service reliability of the bolted joint under transient thermomechanical circumstances. The critical preload 33.5MPa is recommended for the functionally graded bolt studied in this work.

(4) The shape of the nut has a great effect on the stress concentration of the bolt, the nut with an external groove (a/h=1/4, b/l=5/6) can significantly reduce the stress concentration at the first thread of the bolted joint, and thus the reliability of the bolted joint is also improved.

Acknowledgments

The authors are grateful for the support by the National Natural Science Foundation of China (Grant nos. 11090330, 11090331, 11102003 and 11472038), the National Basic Research Program of China (973 Program, 2010CB832701, 2011CB610303), and the Foundation of the Author of National Excellent Doctoral Dissertation of China (No. 201029).

References

[1] Ng, W.H., Friedmann, P.P., and Waas AM, "Thermomechanical Analysis of a Thermal Protection System with Defects and Heat Shorts," *47th AIAA/ASME/ASCE/AHS/ASC Structures, Structural Dynamics, and Materials Conference,* AIAA Paper 2006-2212, Newport, RI, May 2006.

[2] Ng, W.H., McNamara, J.J., Friedmann, P.P., and Waas, A.M, "Thermomechanical Behavior of Damaged TPS Including Hypersonic Flow Effects," *14th AIAA/AHI space planes and hypersonic systems and technologies conference*, AIAA Paper 2006-7951, Canberra, AU, Nov. 2006.

[3] Spinnler, M., Winter, E.R.F., Viskanta, R., and Sattelmayer, T., "Theoretical Studies of High-Temperature Multilayer Thermal Insulations Using Radiation Scaling," *Journal of Quantitative Spectroscopy & Radiative Transfer*, Vol. 84, No. 4, 2004, pp. 477-491.

doi:10.1016/S0022-4073(03)00264-4

[4] Kamran, D., "Thermal analysis and design of multi-layer insulation for re-entry aerodynamic heating," *35th AIAA thermophysics conference*, AIAA Paper 2001-2834, Anaheim, CA, Jun. 2001.

[5] Kondo, N., Suzuki, Y., and Ohji, T., "High-Strength Porous Silicon Nitride Fabricated by the Sinter-Forging Technique," *Journal of Materials Research*, Vol. 16, No. 1, 2001, pp. 32-34.

doi: 10.1557/Jmr.2001.0009

[6] Ortega, F.S., Sepulveda, P., and Pandolfelli, V.C., "Monomer Systems for the Gelcasting of Foams," *Journal of the European Ceramic Society*, Vol. 22, No. 9-10, 2002, pp. 1395-1401.

doi: 10.1016/S0955-2219(01)00486-1

[7] Zhang, G.J., Yang, J.F., and Ohji, T., "Fabrication of Porous Ceramics with Unidirectionally Aligned Continuous Pores," *Journal of the American Ceramic Society*, Vol. 84, No. 6, 2001, pp. 1395-1397.

doi: 10.1111/j.1151-2916.2001.tb00849.x

[8] Yang, L., Liu, Q., Zhou, Y., Mao, W., Lu, C., " Finite Element Simulation on Thermal Fatigue of a Turbine Blade with Thermal Barrier Coatings," *Journal of Materials Science & Technology*, Vol. 30, No. 4, 2014, pp. 371-380.

doi:10.1016/j.jmst.2013.11.005

[9] Liu, T., "Moment-Rotation-Temperature Characteristics of Steel/Composite Connections," *Journal of Structural Engineering*, Vol.125, No. 10, 1999, pp. 1188-1197.

doi: 10.1061/(ASCE)0733-9445(1999)125:10(1188)

[10] Starikov, R., Schön, J., "Quasi-static behaviour of composite joints with countersunk composite and metal fasteners," *Composites: Part B*, Vol. 32, No. 5, 2001, pp. 401-411.

doi:10.1016/S1359-8368(01)00013-0

[11] Ekh, J., Schön, J., Melin, L., "Secondary bending in multi fastener, composite-to-aluminium single shear lap joints," *Composites: Part B*, Vol. 36, No. 3, 2005, pp. 195-208.

doi:10.1016/j.compositesb.2004.09.001

[12] Kabche, J., Caccese, V., Berube, K., Bragg, R., "Experimental characterization of hybrid composite-to-metal bolted joints under flexural loading," *Composites: Part B*, Vol. 38, No. 1, 2007, pp. 66-78.

doi:10.1016/j.compositesb.2006.03.013

[13] Russo, A., Zuccarello, B., "Toward a design method for metal-composite co-cured joints based on the G-SIFs," *Composites: Part B*, Vol. 45, No. 1, 2013, pp. 631-643.

doi:10.1016/j.compositesb.2012.08.024

[14] Wang, H., Yin, H., Qin, S., "Fatigue performance analysis of frictional type high strength bolts of overlapped joints," *13th International Conference on Fracture*, Vol.3, S18-097, Beijing, China, June 2013, pp. 2132-2137.

[15] Marannano, G., Zuccarello, B., "Numerical experimental analysis of hybrid double lap aluminum-CFRP joints," *Composites: Part B*, Vol. 71, Mar. 2015, pp. 28-39.

doi:10.1016/j.compositesb.2014.11.025

[16] Li, G., Zhang, C., Hu, H., Zhang, Y., "Preparation and mechanical properties of C/SiC nuts and bolts," *Materials Science and Engineering a-Structural Materials Properties Microstructure and Processing*, Vol. 547, June 2012, pp. 1-5.

doi:10.1016/j.msea.2012.03.045

[17] Li, G., Zhang, Y., Zhang, C., Hu, H., Chen, S., Zhang, Z., "Design, preparation and properties of online-joints of C/SiC-C/SiC with pins," *Composites: Part B*, Vol. 48, May 2013, pp. 134-139.

doi:10.1016/j.compositesb.2012.09.093

[18] Li, G., Wu, X., Zhang, C., Hu, H., Zhang, Y., Zhang, Z., "Theoretical simulation and experimental verification of C/SiC joints with pins or bolts," *Materials and Design*, Vol. 53, Jan. 2014, pp. 1071-1076.

doi:10.1016/j.matdes.2013.08.001

[19] Hirai, T., Sasaki, M., and Niino, M., "Cvd in-Situ Ceramic Composites, "*Journal of the Society of Materials Science, Japan*, Vol. 36, No. 410, 1987, pp. 1205-1211.

[20] Shi, G., Liang, J., Chen, G., Du, S., "Comparison of tensile properties between NiCoCrAl/YSZ microlaminates and the monolithic NiCoCrAl foil fabricated by EB-PVD," *Materials Letters*, Vol. 63, No. 20, 2009, pp. 1665-1667.

doi:10.1016/j.matlet.2009.04.040

[21] Zhang, R., He, R., Zhou, W., Wang, Y., and Fang, D., "Design and Fabrication of Porous ZrO_2/(ZrO_2+Ni) Sandwich Ceramics with Low Thermal Conductivity and High Strength," *Materials & Design*, Vol. 62, Oct. 2014, pp. 1-6.

doi: 10.1016/j.matdes.2014.05.006

[22] Zhou, W., Zhou H, Zhang, R., Pei Y., Fang, D., "Measuring residual stress and its influence on properties of porous ZrO_2/(ZrO_2+Ni) ceramics," *Materials Science and Engineering a-Structural Materials Properties Microstructure and Processing*, Vol. 622, Jan. 2015, pp. 82-90.

doi:10.1016/j.msea.2014.11.018

[23] Chu, C.L., Zhu, J.C., Yin, Z.D., and Lin, P.H., "Optimal Design and Fabrication of Hydroxyapatite-Ti Asymmetrical Functionally Graded Biomaterial," *Materials Science and Engineering a-Structural Materials Properties Microstructure and Processing*, Vol. 348, No. 1-2, 2003, pp. 244-250.

doi: 10.1016/S0921-5093(02)00738-4

[24] Lee, C.S., Ahn, S.H., DeJonghe, L.C., and Thomas, G., "Effect of Functionally Graded Material (FGM) Layers on the Residual Stress of Polytypoidally Joined Si_3N_4-Al_2O_3," *Materials Science and Engineering a-Structural Materials Properties Microstructure and Processing*, Vol. 434, No. 1-2, 2006, pp. 160-165.

doi: 10.1016/j.msea.2006.06.139

[25] Zang, Z.G., Mukai, K., Navaretti, P., Duelk, M., Velez, C., and Hamamoto, K. "Thermal resistance reduction in high power superluminescent diodes by using active multi-mode interferometer," *Applied Physics Letters*, Vol. 100, No. 031108, 2012, pp. 1-4.

doi:10.1063/1.3678188

[26] Wang, L., Wang, Z., Dong, S.M., Zhang, W., and Wang, Y., "Finite element simulation of stress distribution and development of C_f/SiC ceramic-matrix composite coated with single layer SiC coating during thermal shock," *Composites: Part B*, Vol. 51, August 2013, pp. 204-214.

doi:10.1016/j.compositesb.2013.03.028

[27] Soykok, I.F., Sayman, O., Ozen, M., and Korkmaz, B., "Failure analysis of mechanically fastened glass fiber/epoxy composite joints under thermal effects," *Composites: Part B*, Vol. 45, No. 1, 2013, pp. 192-199.

doi:10.1016/j.compositesb.2012.08.008

[28] Marques, E.A.S., da Silva, L.F.M., and Flaviani, M., "Testing and simulation of mixed adhesive joints for aerospace applications," *Composites: Part B*, Vol. 74, June 2015, pp. 123-130.

doi:10.1016/j.compositesb.2015.01.005

[29] Albedah, A., Bouiadjra, B.B., Aminallah, L., Es-Saheb, M., and Benyahia, F., "Numerical analysis of the effect of thermal residual stresses on the performances of bonded composite repairs in aircraft structures," *Composites: Part B*, Vol. 42, No. 3, 2011, pp. 511-516.

doi:10.1016/j.compositesb.2010.11.013

[30] Parmley, R.O., *Standard Handbook of Fastening and Joining*, 3rd ed., McGraw-Hill, New York, 1980, pp. 1-2.

[31] Pilkey, W.D., *Peterson’s Stress Concentration Factors*, Wiley, New York, 1997, pp. 387-388.

[32] Kingery, W.D., Bowen, H. K, and Uhlmann, D. R., *Introduction to Ceramics*, 2nd ed., John Wiley & Sons, New York, 1976.

[33] Kondo, R., *Porous Materials*, Gihoudo, Tokyo, 1986.

[34] Zhang, X.C., Xu, B.S., Wang, H.D., Jiang, Y., and Wu, Y.X., "Application of Functionally Graded Interlayer on Reducing the Residual Stress Discontinuities at Interfaces within a Plasma-Sprayed Thermal Barrier Coating," *Surface & Coatings Technology*, Vol. 201, No. 9-11, 2007, pp. 5716-5719.

doi: 10.1016/j.surfcoat.2006.07.062

[35] RoyMech, "Friction Coefficient Bolted Joints," <http://www.roymech.co.uk/Useful_Tables/Tribology/co_of_frict.htm>.

[36] Yang, S., Tao, W., *Heat Transfer*, 4th ed., Higher Education Press, Beijing, 2006.

[37] Venkatesan, S., Kinzel, G.L., "Reduction of stress concentration in bolt-nut connectors," *Journal of Mechanical Design*, Vol. 128, No. 6, 2006, pp. 1337-1342.

doi:10.1115/1.2336254

Figures and Tables

Table 1 Temperature-dependent material parameters for porous ZrO_2/(ZrO_2+Ni) FGMs

Temperature(°C)		25	300	600	800	1000	1127
ZrO_2	E(GPa)	198.67	187.82	166.76	149.73	131.23	118.94
	λ(W/(m·K))	2.22	2.06	2.02	2.08	2.20	2.31
ZrO_2 (30% porosity)	E(GPa)	115.43	109.13	96.89	86.99	76.24	69.11
	α(10^{-6}/K)	8	8.60	9.20	9.60	10	10.254
	λ(W/(m·K))	0.810	0.800	0.790	0.793	0.811	0.833
	C(J/kg·K)	473.3	594.3	643	707.6	854.2	1012.0
Ni	E(GPa)	205	204.81	176.82	158.16	139.50	127.65
	α(10^{-6}/K)	12.73	16.45	17.93	19.15	21.07	22.51
	λ(W/(m·K))	92.465	68.335	68.199	73.430	78.370	80.317
	C(J/kg·K)	426.1	576.9	528.1	460.6	362.6	295.4
ZrO_2+15%Ni (15% porosity)	E(GPa)	153.88	146.75	129.72.	116.39	102.12	92.70
	α(10^{-6}/K)	8.71	9.78	10.51	11.03	11.66	12.09
	λ(W/(m·K))	2.126	2.017	1.999	2.032	2.118	2.190
	C(J/kg·K)	466.2	591.7	625.8	670.5	780.7	904.5
ZrO_2+30%Ni (12% porosity)	E(GPa)	163.08	156.85	138.04	123.79	108.72	98.83
	α(10^{-6}/K)	9.41	10.95	11.82	12.46	13.32	13.93
	λ(W/(m·K))	3.145	3.039	3.020	3.054	3.141	3.216
	C(J/kg·K)	459.1	589.1	608.5	633.5	706.7	797.0
	σ_t(MPa)	159	158.7	158.5	115.5	85.5	66.4
	h_f(W/(m^2·K))	-	-	19.15	44.15	84.71	115.24

(E: elastic modulus, λ: thermal conductivity, α: CTE, C: specific heat, σ_t: tensile strength, h_f: convection and radiation coefficient)

Table 2 Temperature-independent material parameters for porous ZrO_2/(ZrO_2+Ni) FGMs

	ZrO_2	Ni	ZrO_2 (30% porosity)	ZrO_2+15%Ni (15% porosity)	ZrO_2+30%Ni (12% porosity)
μ	0.315	0.3	0.315	0.313	0.311
ρ(kg/m^3)	5650	8902	5650	6137	6625

(μ: Poisson's ratio, ρ: density)

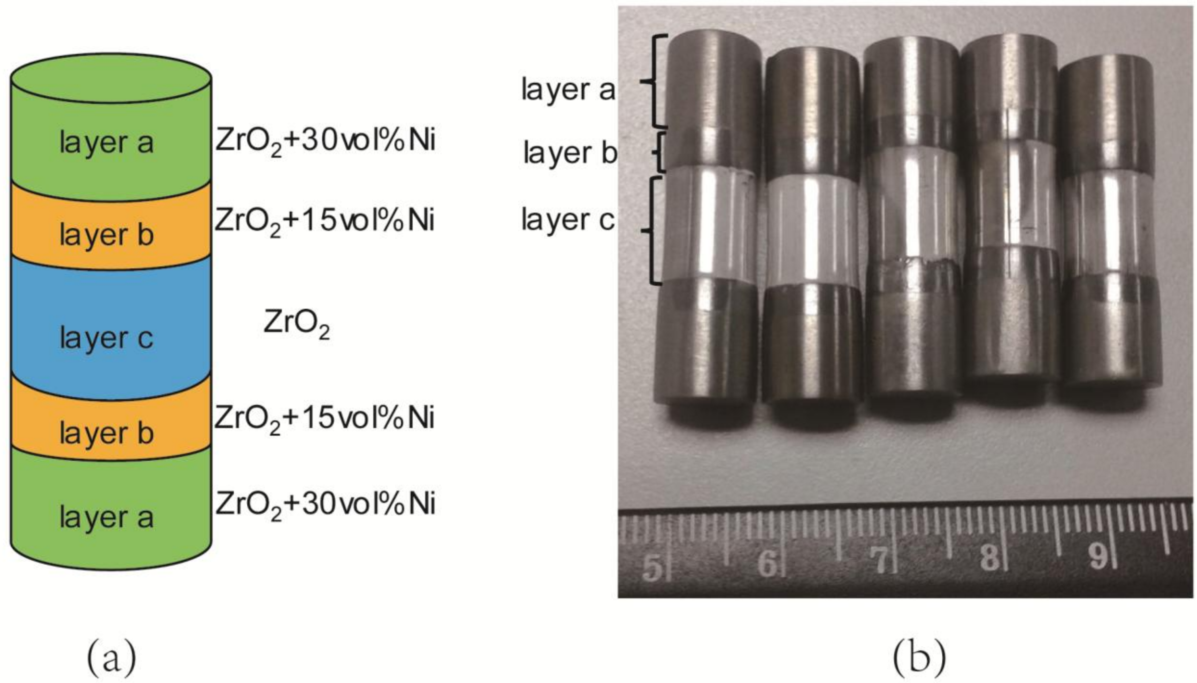

Fig.1 Schematic composition and optical photograph of the fabricated porous ZrO_2/(ZrO_2+Ni) FGMs. a), b)

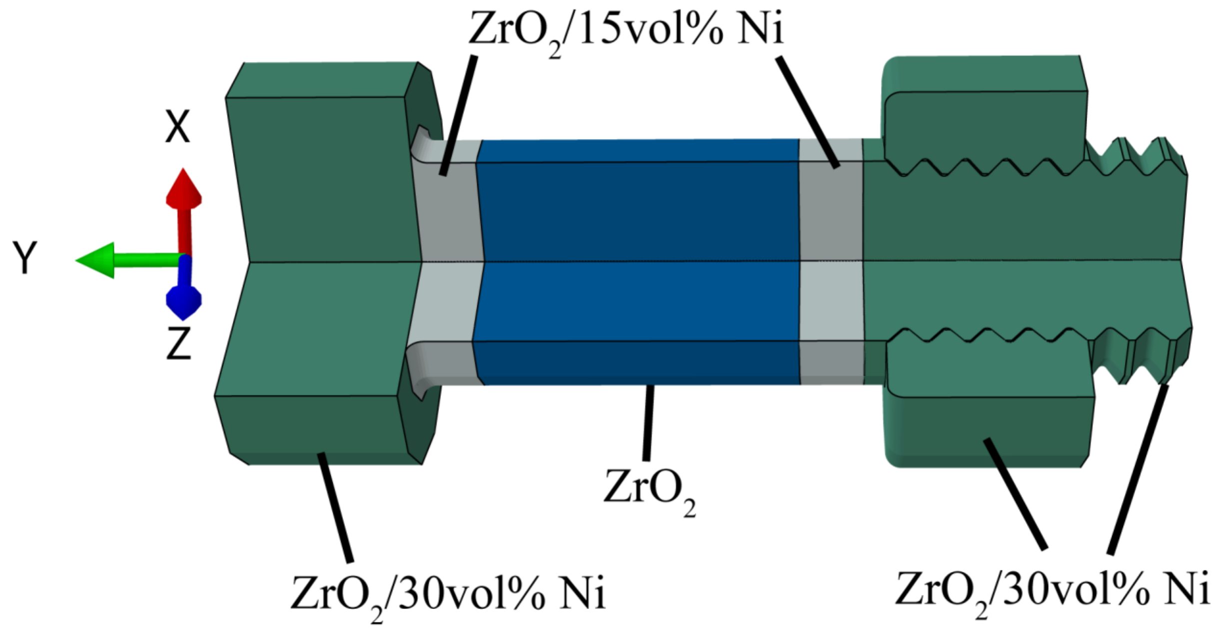

Fig.2 **Illustration of the materials and structure of the functionally graded bolted joint.**

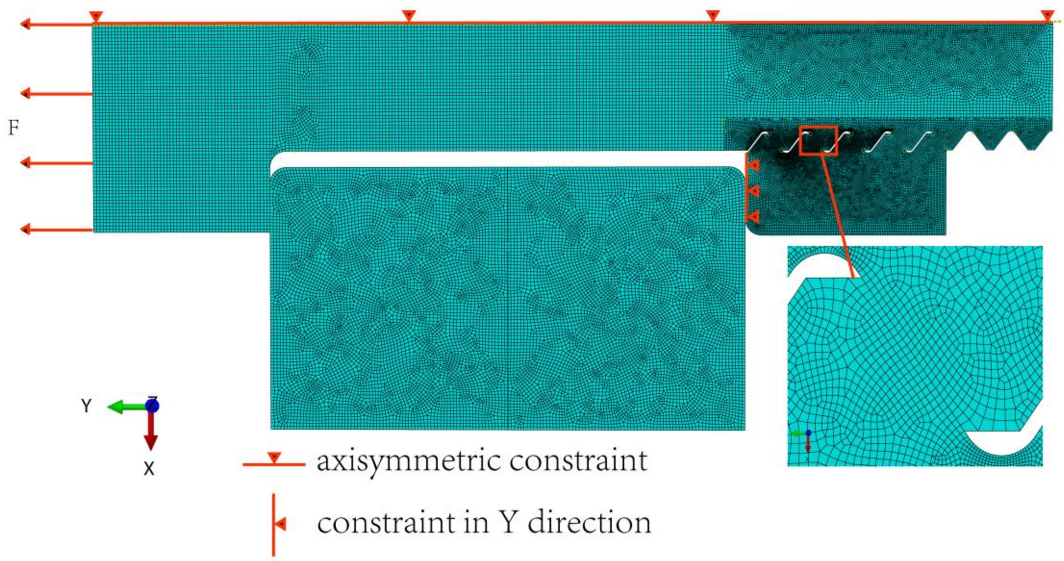

Fig.3 **Illustration of the finite element model of the functionally graded bolted joint.**

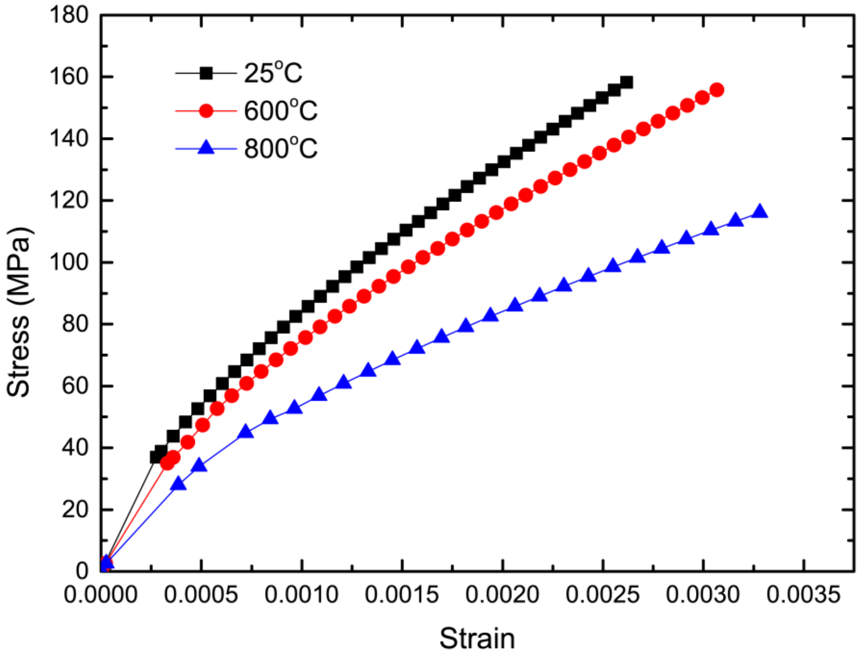

Fig.4 Tension experiments of the porous ZrO_2/(ZrO_2+Ni) FGMs

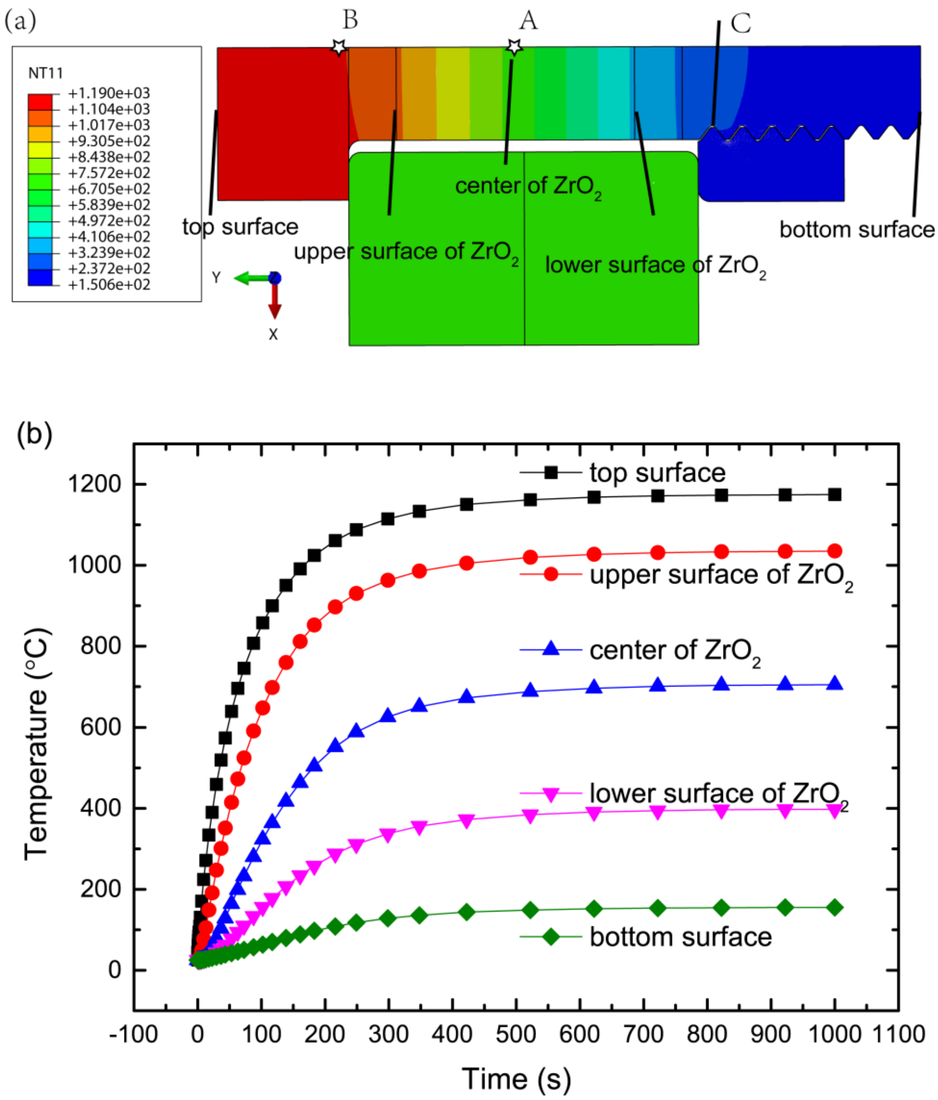

Fig.5 (a) Temperature contour of the functionally graded bolted joint at the end of the heat transfer process (t=1000s), (b) Temperature history of the functionally graded bolted joint at different locations.

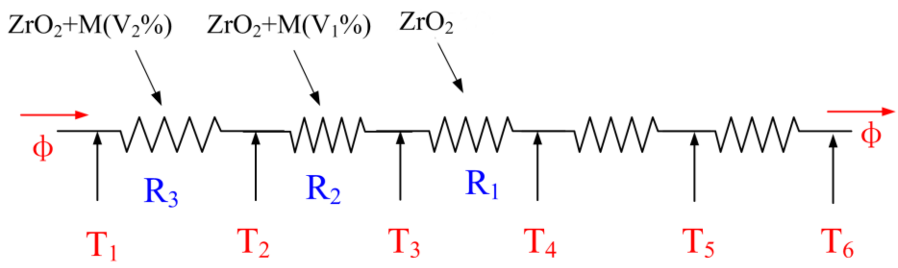

Fig.6 The equivalent heat resistance schematic of the functionally graded bolted joint in the height direction.

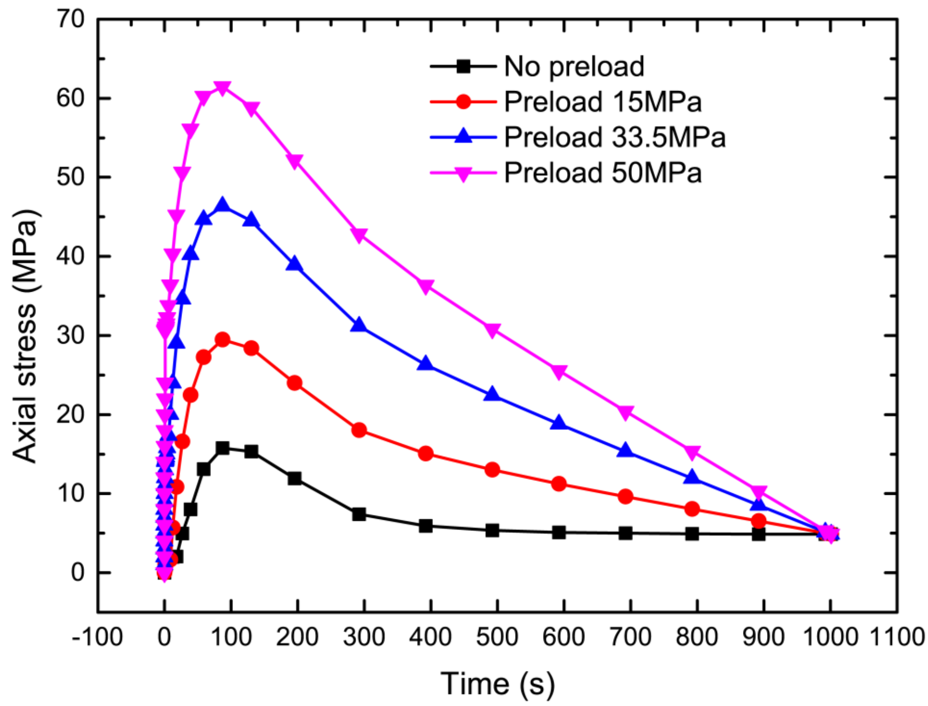

Fig.7 The axial stress-loading time curves of location A (center of the ZrO_2 layer) of the functionally graded bolted joint.

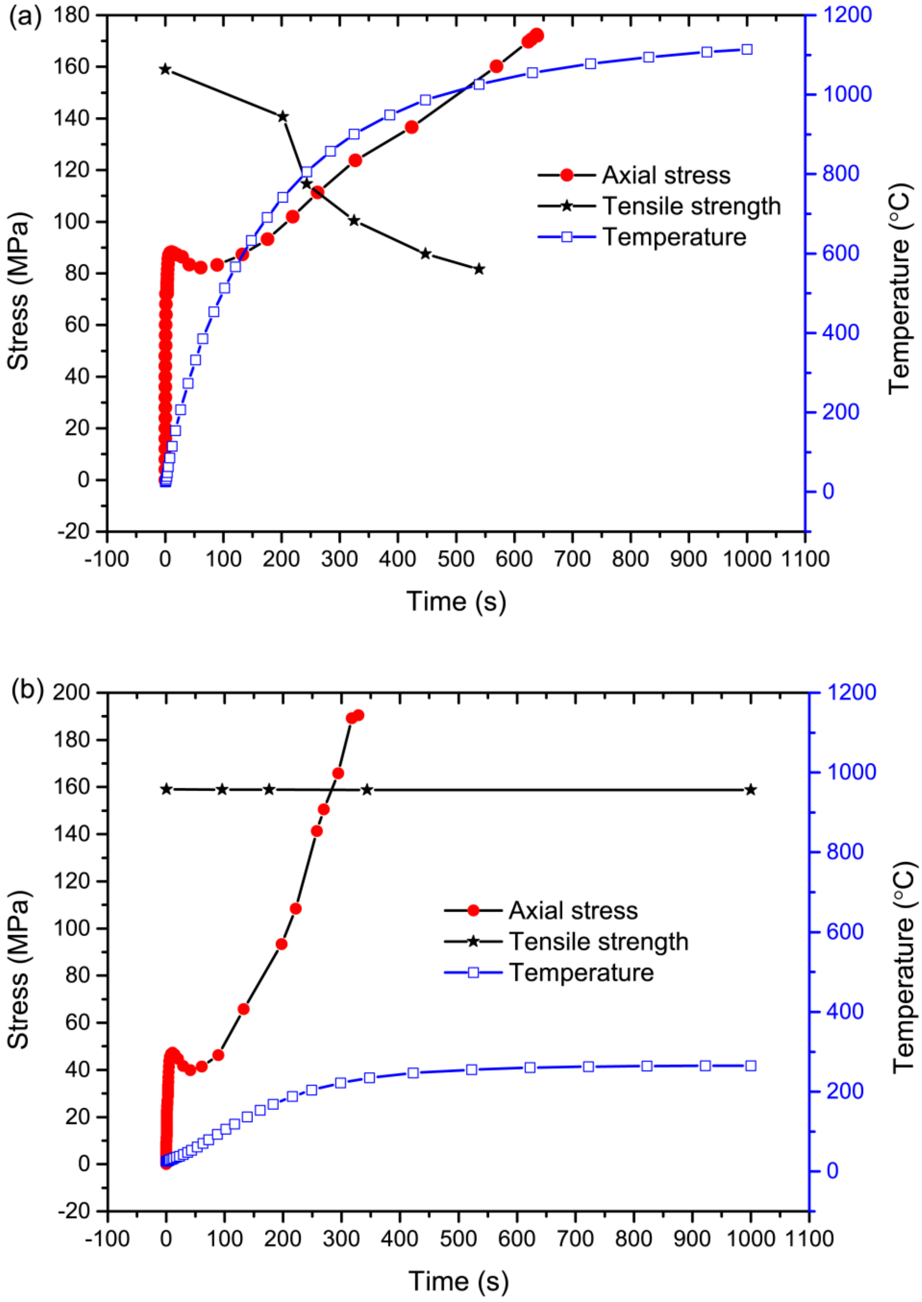

Fig.8 Axial stress-loading time curves under the preload (15MPa): (a) location B, (b) location C.

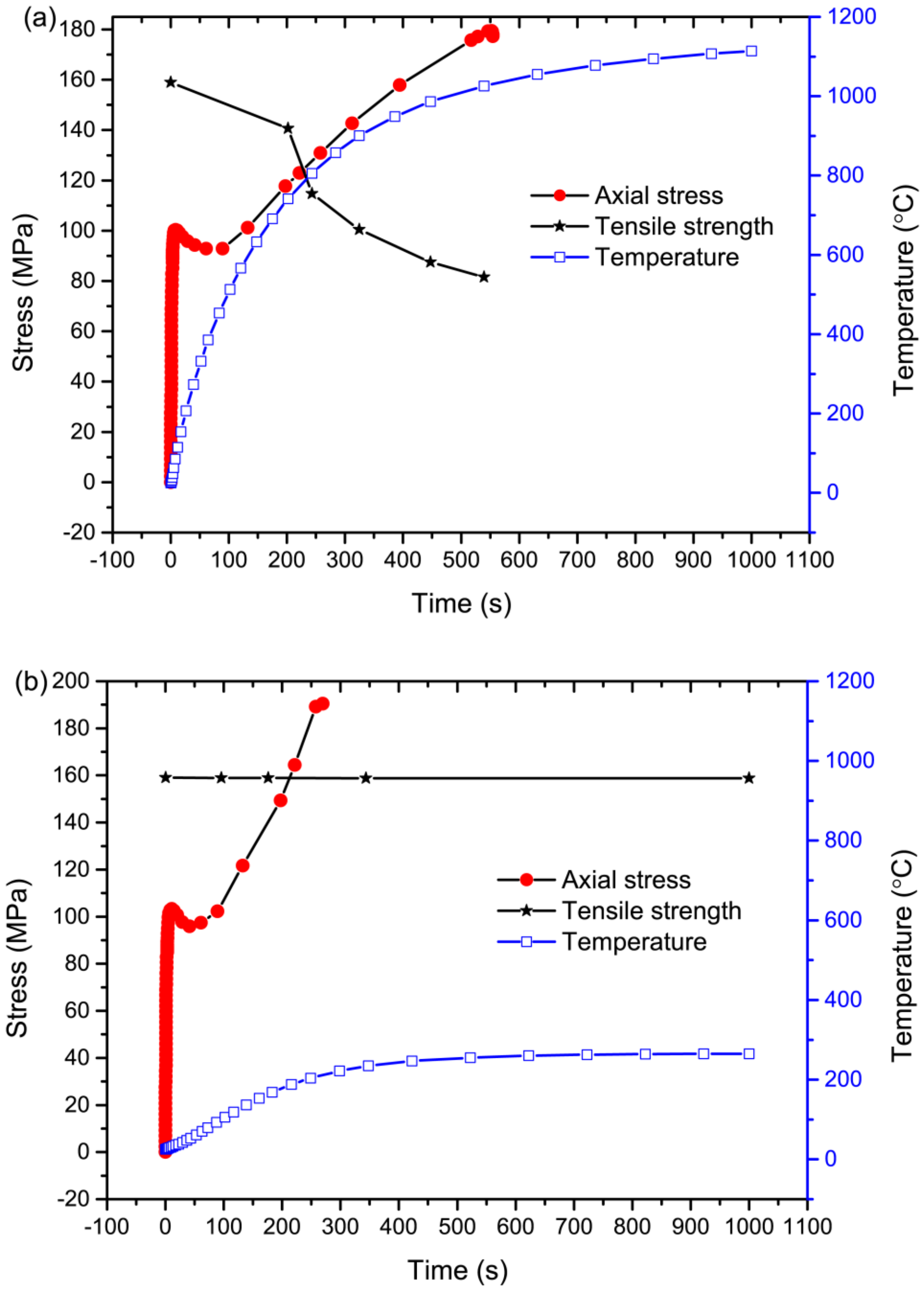

Fig.9 Axial stress-loading time curves under the preload (33.5MPa): (a) location B, (b) location C.

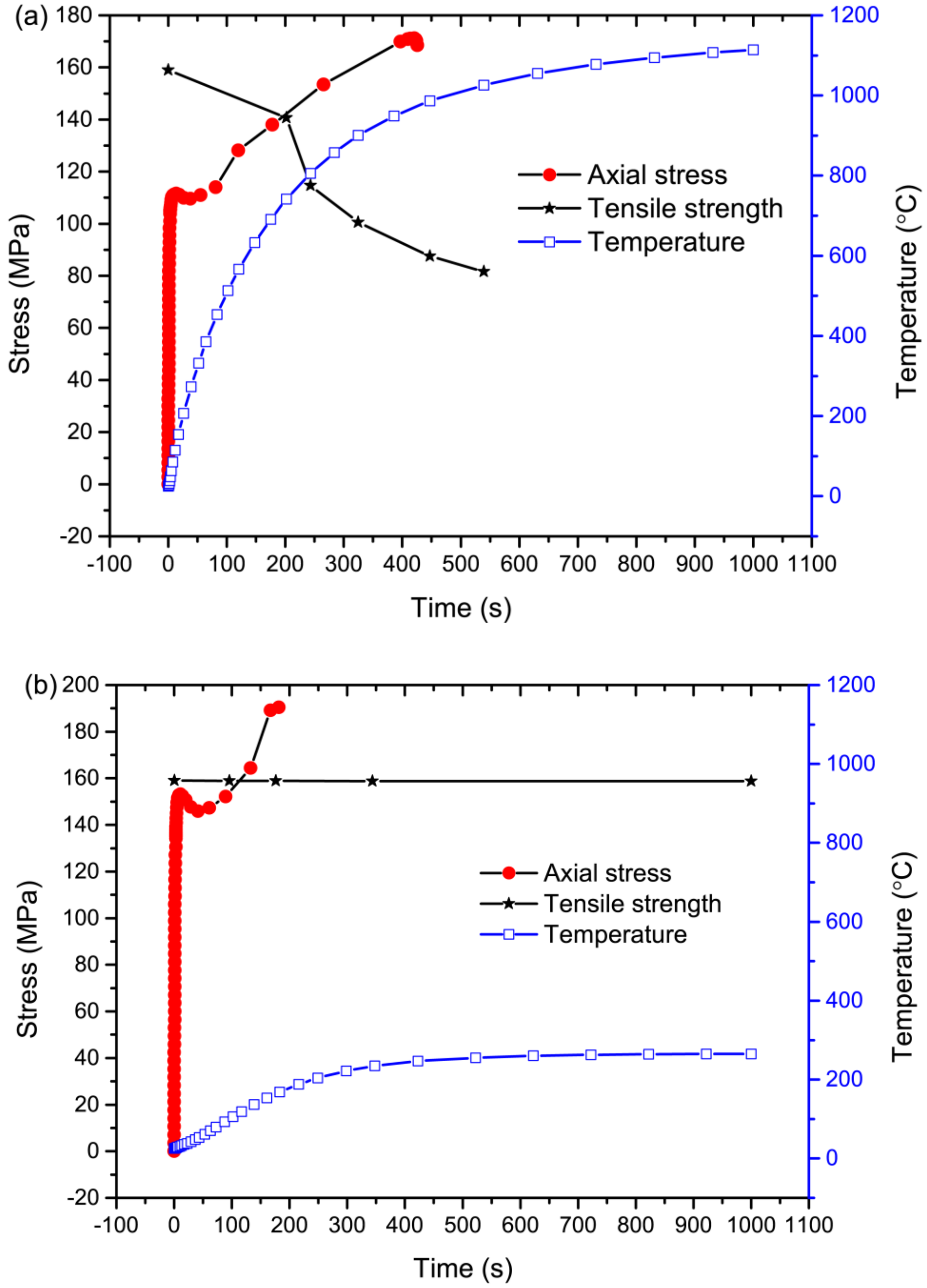

Fig.10 Axial stress-loading time curves under the preload (50MPa): (a) location B, (b) location C.

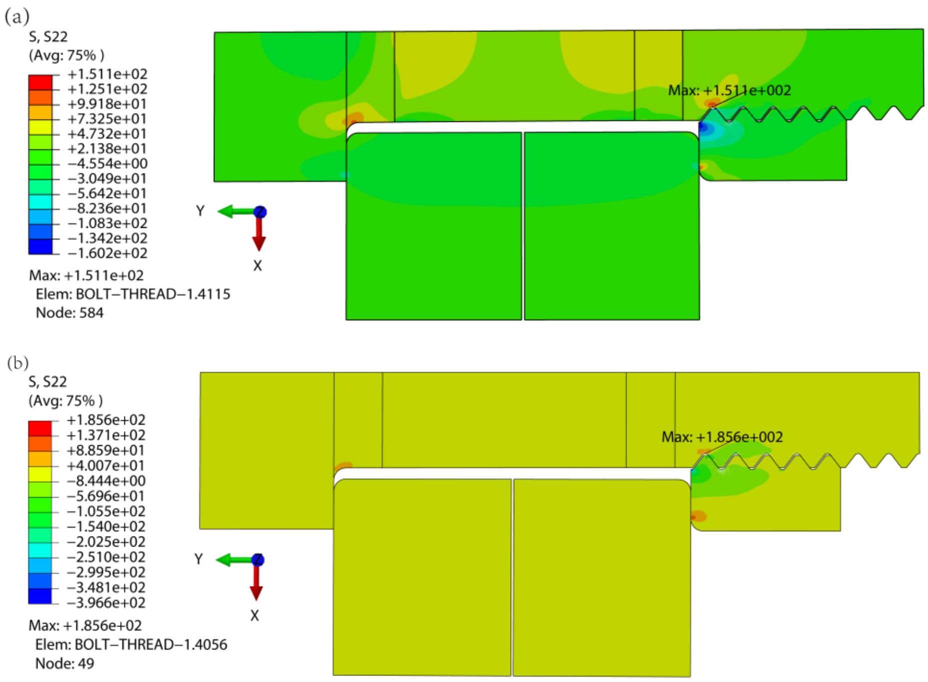

Fig.11 The axial stress profile of the bolted joint at the end of the thermomechanical process: (a) functionally graded bolt, (b) ZrO_2 ceramic bolt.

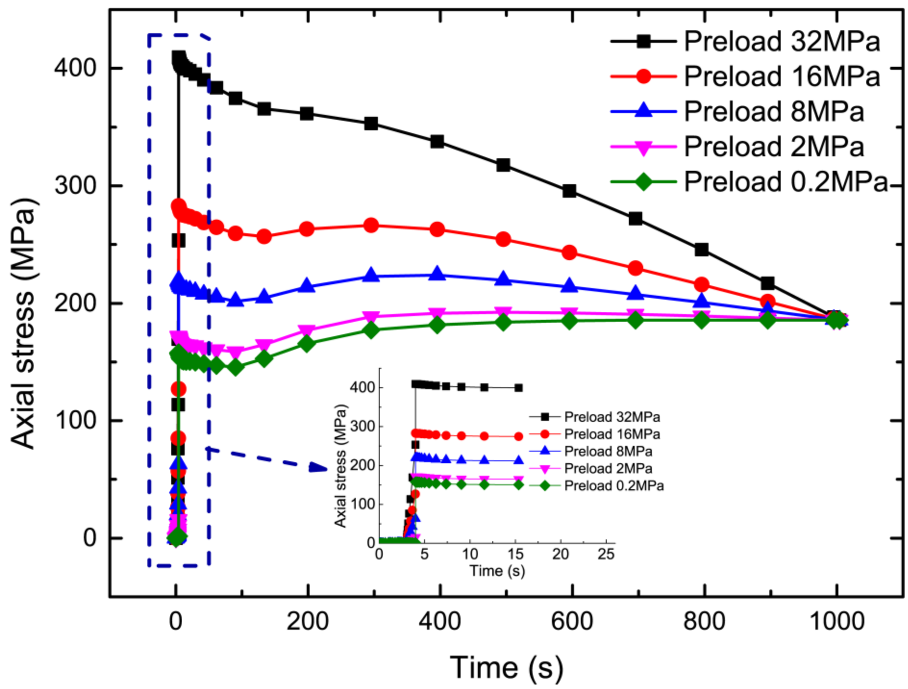

Fig.12 The axial stress-loading time curves of the root of the first thread of the ZrO_2 ceramic bolt under different preloads

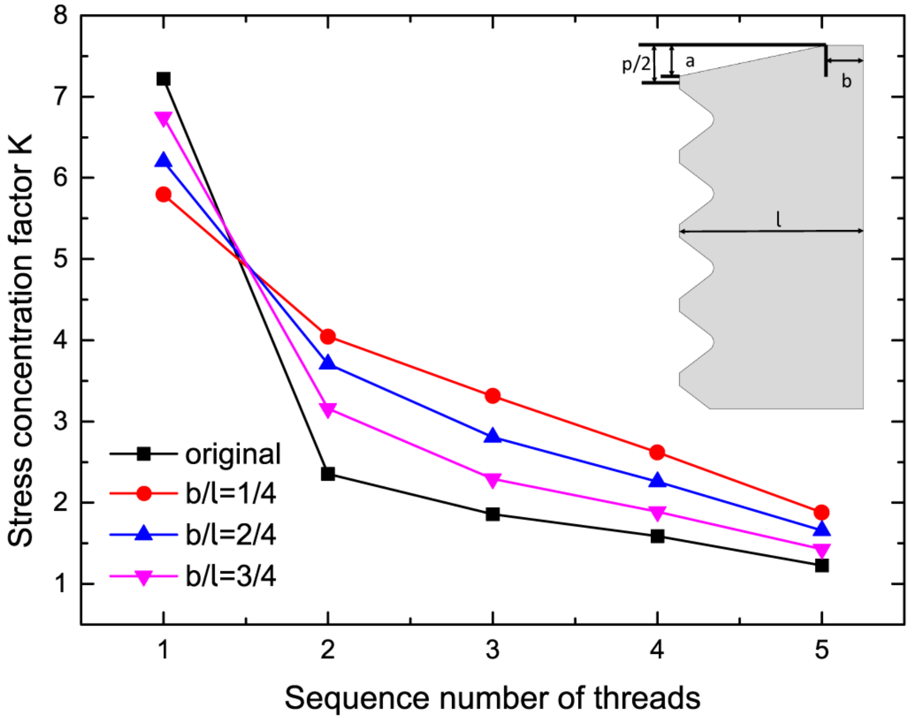

Fig.13 Influences of the internal groove on the stress concentration factor of threads of the functionally graded bolt.

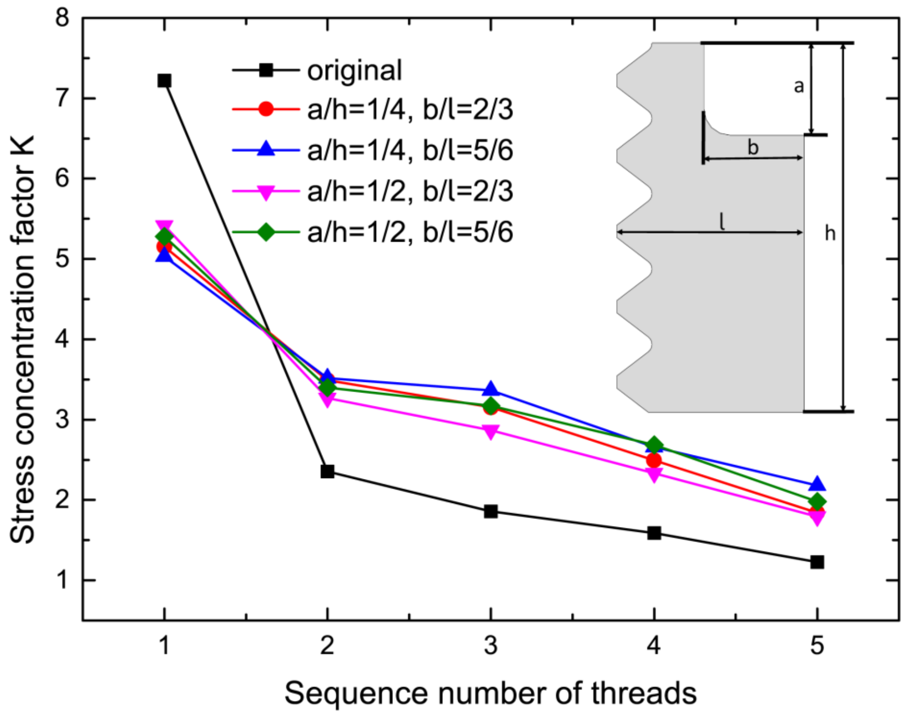

Fig.14 Influences of the external groove on the stress concentration factor of threads of the functionally graded bolt.